ELSEVIER

Surface Science 411 (1998) 186–202

surface science

The surface energy of metals

L. Vitos [a], A.V. Ruban [a], H.L. Skriver [a,]*, J. Kollár [b]

[a] *Center for Atomic-scale Materials Physics and Department of Physics, Technical University of Denmark, DK-2800 Lyngby, Denmark*
[b] *Research Institute for Solid State Physics, H-1525 Budapest, P.O. Box 49, Hungary*

Received 3 November 1997; accepted for publication 2 May 1998

Abstract

We have used density functional theory to establish a database of surface energies for low index surfaces of 60 metals in the periodic table. The data may be used as a consistent starting point for models of surface science phenomena. The accuracy of the database is established in a comparison with other density functional theory results and the calculated surface energy anisotropies are applied in a determination of the equilibrium shape of nano-crystals of Fe, Cu, Mo, Ta, Pt and Pb. © 1998 Elsevier Science B.V. All rights reserved.

Keywords: Ab initio quantum chemical methods and calculations; Density functional calculations; Green's function methods; High index single crystal surfaces; Low index single crystal surfaces; Metals; Single crystal surfaces; Surface energy

1. Introduction

The surface energy γ defined as the surface excess free energy per unit area of a particular crystal facet is one of the basic quantities in surface physics. It determines the equilibrium shape of mezoscopic crystals, it plays an important role in faceting, roughening, and crystal growth phenomena, and may be used to estimate surface segregation in binary alloys. Most of the experimental surface energy data [1,2] stems from surface tension measurements in the liquid phase extrapolated to zero temperature. Although these data at present form the most comprehensive experimental source of surface energies they include uncertainties of unknown magnitude and correspond to an isotropic crystal. Hence, they do not yield information as to the surface energy of a particular surface facet. Except for the classic measurements on Pb and In [3,4] there are to our knowledge no direct experimental determinations of the anisotropy in the surface energy of solids. A theoretical determination of the surface energy is therefore of vital importance.

During the last decade there have been many calculations of the surface energy of metals either from first-principles [5–7] or by semi-empirical methods [8]. The latter are of course computationally highly efficient and in many cases provide a good description of the energetics of surfaces. Hence, they have been used with great success to study and understand trends. In contrast, most first-principles methods are computationally demanding and have typically been used only for particular cases, focusing on a few elements or on a special application for a given metal surface. However, recently Methfessel et al. [5] have used

---

* Corresponding author. Tel.: (+45) 45 88 24 88; fax: (+45) 45 93 23 99; e-mail: skriver@fysik.dtu.dk

PII: S0039-6028(98)00363-X

the full potential linear muffin-tin orbitals (LMTO) method to investigate the trends in the surface energy, work function, and surface relaxation in the bcc and fcc 4d transition metals. Concurrently, Skriver and co-workers [6,7,9,10] used the Green's function LMTO method [11] in the atomic-sphere approximation (ASA) to calculate the surface energy and work function of most of the elemental metals including the light actinides. In all of these first-principles calculations little attention has been paid to the dependence of the surface energy on the orientation of the surface facets and hence there is at present no comprehensive first-principles database for surface energy anisotopies. It is the aim of the present paper to fill this gap.

Our starting point is the well-established fact that density functional theory (DFT), either in the local density approximation (LDA) or the generalized gradient approximation (GGA), yields ground state properties of metals in close agreement with experimental observations. Hence, by using the LDA and GGA for all metals in the periodic table we should be able to form a consistent and accurate database of surface energies including the anisotropies for which there are few experimental observations. Given the LDA or the GGA we need to be able to solve the one-electron problem accurately and efficiently if we are to cover most of the periodic table for a multitude of surface facets. To this end we apply the recently developed full charge density (FCD) LMTO method [12,13] which was shown to have an accuracy comparable with that of the full potential methods. To establish the accuracy for the present purpose we compare our surface energies for the 4d transition metals with the full potential calculations [5] and find close agreement between the two sets of results. We therefore expect our calculated database of surface energies to reflect the true DFT result.

2. Computational method

A full description of the FCD method may be found in Refs. [13–15]. Here, we outline the important numerical details and establish the accuracy of the FCD approach through a comparison with other first-principles LDA calculations. We further calculate the surface energies of the 4d metals in the LDA as well as the GGA assuming a close packed fcc (111) surface and compare the results with the isotropic experimental results [2].

2.1. Full charge density scheme for surfaces

The FCD method is based on density functional theory [16]. The Kohn–Sham one-electron equations are solved by means of the extremely efficient tight-binding LMTO method in the ASA [17–20]. The complete non-spherically symmetric charge density $n(\mathbf{r})$ is constructed from the output of a self-consistent Green's function LMTO-ASA calculation and normalized within space-filling non-overlapping cells centered around each atomic site. The total density so constructed is continuous and continuously differentiable in all space [15]. It was shown by Andersen et al. [21] that the full charge density obtained on the basis of a spherically symmetric self-consistent calculation is close to the density obtained using a full potential method even for open structures such as diamond. Therefore, we expect the total energy functional evaluated from the full charge density derived by an LMTO-ASA calculation to be a very good approximation to the total energy of the system.

The Hartree and exchange-correlation parts of the FCD energy functional $E^{\mathrm{FCD}}[n]$ are calculated exactly from the charge density $n(\mathbf{r})$ using the LDA or GGA exchange-correlation energy functionals, while the kinetic energy is given by the Kohn–Sham kinetic energy obtained from the LMTO-ASA equations corrected by a term due to the non-spherically symmetric part of the charge density neglected in the self-consistency procedure. This correction is evaluated in terms of a gradient expansion around the spherically symmetric charge density using the functional form for the kinetic energy of noninteracting particles [16], as described in Ref. [13]. Thereby, the FCD method retains most of the simplicity and the computational efficiency of the LMTO-ASA method, but attains an accuracy comparable with that of the full potential methods as demonstrated in the successful calculations of the bulk ground state properties, including the shear elastic constants, for the 4d transition metals and the equilibrium volumes of the α-phases of the light 5f metals [12,13,22].

In the application of the FCD method to surface energy calculations the one-electron equations are solved by means of the surface Green's function technique developed by Skriver and Rosengaard [11]. The method correctly accounts for the semi-infinite nature of a surface by means of the principal layer technique [23]. The Dyson equation describing the relaxation of the electronic structure of the surface region is set up and solved within the atomic sphere approximation, taking into account the electrostatic mono- and dipole contributions to the spherically symmetric one-electron potential [11]. In the present implementation the relaxation of the surface atomic positions is neglected. According to the first-principles works by Feibelman et al. [24,25] and by Mansfield et al. [26] the effect of relaxation on the calculated surface energy of a particular crystal facet may vary from 2 to 5% depending on the roughness. The semi-empirical results by Rodriguez et al. [8] show that surface relaxation typically affects the anisotropy by less than 2% and therefore the neglect of relaxations in the present work has little effect on the accuracy of the calculated database.

Since the surface one-electron potential includes the electrostatic dipole contribution, the Kohn–Sham kinetic energy obtained within the ASA implicitly contains the main effect of the semi-infinite surface [11]. For close packed surfaces the ASA kinetic energy is therefore a good approximation to the exact kinetic energy. In the surface FCD calculations the nonspherical correction to the ASA surface kinetic energy is estimated by means of a second-order gradient expansion of the kinetic energy functional [16]. The actual calculations show that this correction becomes important only for open surfaces and that in most cases only densities of low gradients are involved. Hence, although a density gradient expansion does not in general work for the complete kinetic energy we find that it works well for the correction to the ASA kinetic energy.

At zero temperature the surface excess free energy may be calculated as the difference

$$\gamma = E_{2D}^{FCD}(N_a + N_v) - N_a E_{3D}^{FCD} \qquad (1)$$

between the total energy of N_a atoms plus N_v empty spheres in the surface region (2D) and N_a times the total energy per atom in the bulk (3D). This approach is purely semi-infinite and does not rely on a slab or supercell geometry. Further, to reduce numerical errors the total energy of the bulk E_{3D}^{FCD} is evaluated by means of a Green's function technique similar to that used in the surface FCD calculations, i.e., all one-electron quantities are obtained by contour integrals of Green's functions rather than by a conventional Hamiltonian eigenvalue technique.

2.2. *Numerical details*

In all calculations the one electron equations were solved within the scalar-relativistic and frozen-core approximations. In the LMTO basis set we included sp and d orbitals in the case of the simple metals, and spd and f orbitals in the case of transition metals and light actinides including Fr and Ra. For In the 4d, for Tl and Pb the 5d, and for the light actinides the 6p states were treated as band states using a second energy panel. The valence electrons were treated self-consistently in the local density approximation with the Perdew–Wang parametrization [27] of the results of Ceperley and Alder [28] for exchange and correlation and to obtain the total energy in the generalized gradient approximation the FCD functional included the exchange-correlation functional given by Perdew et al. [29].

The Dyson equation for the bulk and surface calculations was solved for 16 complex energy points distributed exponentially on a semicircular contour. The *k*-point sampling in the bulk calculations was performed on a uniform grid, while in the surface calculations special *k*-points were used [30]. The number of *k*-points in the irreducible wedge of the 3D and 2D Brillouin zones for each structure and surface orientation are shown in Table 1. The hcp structure has two $(10\bar{1}0)$ surfaces depending on the first interlayer distance d^{-10}, and in the table $(10\bar{1}0)_A$ refers to the surface with $d_A^{-10} = (\sqrt{3}/6)a$ while $(10\bar{1}0)_B$ denotes the surface with $d_B^{-10} = 2d_A^{-10}$. In the calculations the numbers of atomic layers were chosen such that the relative error in the surface energy caused by the difference between the energy of the deepest lying atomic

Table 1
Number of *k*-vectors in the irreducible wedge of the three dimensional (3D) and the two dimension (2D) Brillouin zones and number of atomic (N_a) and vacuum (N_v) layers used in the self-consistent calculations. A_{2D} is the area of the 2D unit cell and a and c are lattice parameters

Structure	$N_k^{\mathrm{IBZ-3D}}$	Surface	A_{2D}	2D Brillouin zone	$N_k^{\mathrm{IBZ-2D}}$	N_a	N_v
fcc	505	(111)	$\sqrt{3}/4a^2$	hexagonal	45	4	2
		(100)	$1/2a^2$	square	36	4	2
		(110)	$\sqrt{2}/2a^2$	rectangular-P	64	6	3
bcc	506	(110)	$\sqrt{2}/2a^2$	rectangular-C	64	6	2
		(100)	a^2	square	36	6	3
		(211)	$\sqrt{3/2}a^2$	rectangular-P	128	8	4
		(310)	$\sqrt{10}/2a^2$	rectangular-C	128	8	4
		(111)	$\sqrt{3}a^2$	hexagonal	45	8	4
hcp	225	(0001)	$\sqrt{3}/2a^2$	hexagonal	45	4	2
		$(10\bar{1}0)_A$	$\sqrt{8/3}a^2$	rectangular-P	64	8	4
		$(10\bar{1}0)_B$	$\sqrt{8/3}a^2$	rectangular-P	64	8	4
bct	594	(001)	a^2	square	36	4	2
		(110)	$\sqrt{2}/2ac$	rectangular-C	64	4	2
		(100)	ac	rectangular-P	64	4	4
sc	455	(100)	a^2	square	36	4	2
		(110)	$\sqrt{2}a^2$	rectangular-P	64	6	3

layer and the bulk energy was less than 1%. The actual numbers of atomic (N_a) and vacuum layers (N_v) used are shown in the last two columns of Table 1.

The electronic charge density was represented in an one-center expansion in terms of spherical harmonics including terms up to $l_{\max}=10$ and the normalization of the charge density was ensured by the technique described in Section IIA of Ref. [14]. The FCD energy functional was evaluated by means of the shape function technique using a linear radial mesh between the inscribed and circumscribed spheres. The conventional Madelung terms were calculated up to $l_{\max}=8$. For the nearest neighbor cell interaction we used the technique described in Refs. [14,31] taking $l_{\max}=30$ for the multipole moments.

2.3. Comparison with full-potential LDA calculations

To establish the accuracy of the present method for metal surfaces we may compare our calculated surface energies with other first-principles results. To our knowledge, the only systematic calculation of the surface energy of a transition metal series and of the corresponding surface energy anisotropy is carried out by Methfessel et al. [5] in their full potential (FP) LMTO study of the 4d metals. For the close packed fcc (111) surfaces the comparison between the results obtained by these two methods have been presented in Ref. [14], where we found a 10% mean deviation in the surface energy over the 4d series. The present implementation of the FCD method, using the same basis set and the same exchange-correlation functional as the full potential calculation, gives a mean deviation for the closed packed surfaces similar to that found in Ref. [14].

The accuracy of the orientation dependence of the surface energy may be assessed from Fig. 1 where we compare the FCD anisotropy ratios $\gamma_{100}/\gamma_{111}$ and $\gamma_{110}/\gamma_{111}$ for the 4d transition metals assuming the fcc structure for the whole series with those obtained in the FP-LMTO calculations by Methfessel et al. [5]. We note that $\gamma_{100}/\gamma_{111}$ and $\gamma_{110}/\gamma_{111}$ in the nearest neighbor broken bond model are 1.15 and 1.22, respectively and that the first-principles results shown in the figure deviate somewhat from these values. In particular, the

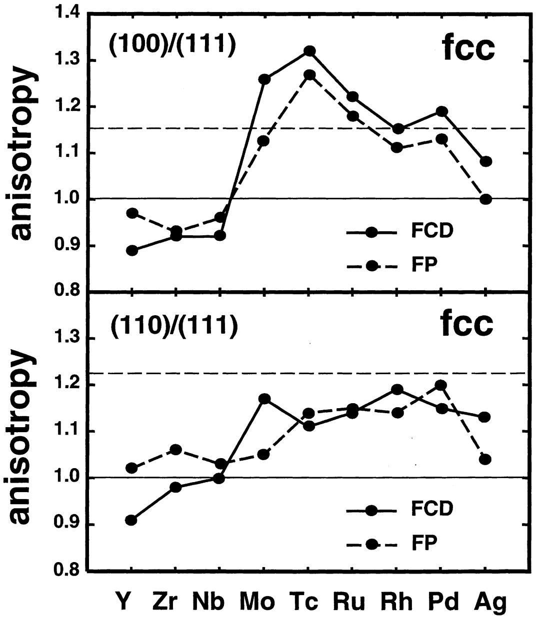

Fig. 1. Comparison of the FCD surface energy anisotropies for the low index fcc surfaces of the 4d elements with the full-potential slab calculation by Methfessel et al. [5]. The thin dashed lines indicate the values obtained in the nearest neighbor broken bond model. Note that the results shown in the figure are LDA results calculated for comparison only. They are approximately 1% larger than the corresponding GGA results listed in Table 6.

elements Mo–Pd exhibit an increased $\gamma_{100}/\gamma_{111}$ but a reduced $\gamma_{110}/\gamma_{111}$ relative to the broken bond model. This may be explained in terms of the pair-potential expansion, to be introduced in Section 4. In this expansion the next-nearest neighbor potentials are negative which, coupled with the fact that the number of broken next-nearest neighbor bonds for the (100) and the (110) surfaces is 2 and 4, respectively, leads to the deviations from the nearest neighbor broken bond model observed in Fig. 1 for Mo–Pd.

In the comparison one should note that the full potential calculations rely on a slab supercell geometry with 7 metallic layers which may be insufficient for the open surfaces[1], are non-relativistic, and allow the atomic positions at the surface to relax while the present Green's function technique describes a single semi-infinite surface, is scalar relativistic, and does not include relaxation of atomic positions. Further, the full potential calculations utilize a triple spd basis while the present calculations utilize a single basis but include the f orbitals as well. Finally, the full potential method makes use of the Perdew–Zunger parametrization [32] of the results of Ceperley and Alder [28] for the exchange-correlation functional while the present FCD method, for this comparison only, uses the Perdew–Wang parametrization [27] of the same results. With these differences in mind the agreement between the two calculations is very good, the mean deviations for $\gamma_{100}/\gamma_{111}$ and $\gamma_{110}/\gamma_{111}$ for the fcc surfaces over the 4d period being around 5% and 6%, respectively.

The largest deviation between the two sets of calculations is found in Mo where an anomalous surface relaxation causes a substantial reduction in the surface energy of the (100) and (110) facets in the full potential calculations. However, Mo forms in the bcc structure and for this the two methods yields $\gamma_{100}/\gamma_{110}$ values that agree within 1%. For the other bcc metal Nb our anisotropy is substantially lower than that obtained in the full potential LMTO calculation but in this case the full potential linear augmented plane wave (LAPW) calculation by Weinert et al. [33] gives $\gamma_{100}/\gamma_{110} = 1.07$ which compares well with our value of 1.06 and with the similarly low anisotropy we find for V and Ta (see Section 3.2).

2.4. *LDA versus GGA*

The most significant assumption in the FCD calculations is the approximate functional form for the exchange and correlation energy. In most density functional calculations some form of local density approximation is used with great success to describe ground state properties of a wide range of bulk and surface systems. For surfaces the accuracy of the LDA was studied within the self-consistent jellium surface model by Perdew et al. [34], and good agreement was found with the

---

[1] To obtain convergence we use in the present calculations from 4 to 8 metallic layers, see Table 1, which have the correct boundary condition at the vacuum and bulk interfaces. A similar convergence in terms of the number of metallic layers in a slab supercell method needs approximately 8 to 16 metallic layer.

experimental result[2], especially for slowly varying density profiles. Its success was ascribed to a cancellation between the errors in the exchange and correlation energies. The gradient correction to the LDA [29,34] represents an important improvement for the correlation part, but it underestimates the exchange energy, and as a consequence it gives surface energies which are 7–16% lower than the LDA values for jellium and 16–29% lower than the experimental results [34]. On these grounds one may therefore prefer the LDA results in the database. However, since the study by Perdew et al. of the validity of the LDA and GGA for surfaces is based on the jellium model which at best is only applicable to simple metals one needs to compare surface energies obtained for a larger range of real metals before judging the relative merits of the two approximations to density functional theory.

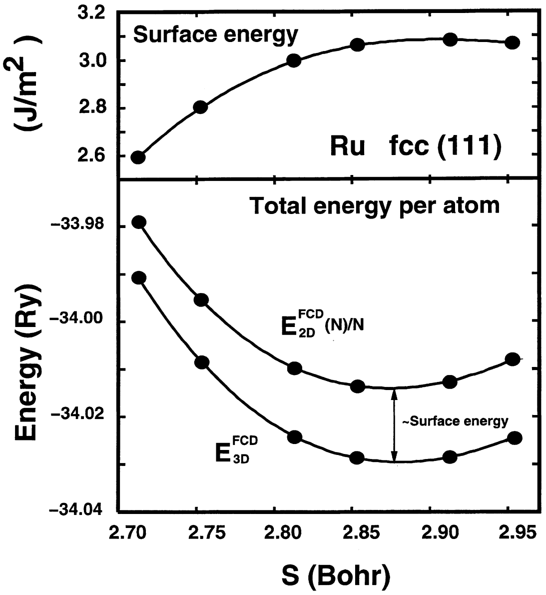

Fig. 2. Upper panel: surface energy versus Wigner–Seitz radius for a Ru fcc (111) surface. Lower panel: total energy per atom versus Wigner–Seitz radius for bulk ($E^{\rm FCD}_{\rm 3D}$) and for the atoms in the surface region ($E^{\rm FCD}_{\rm 2D}(N)/N$) for fcc Ru.

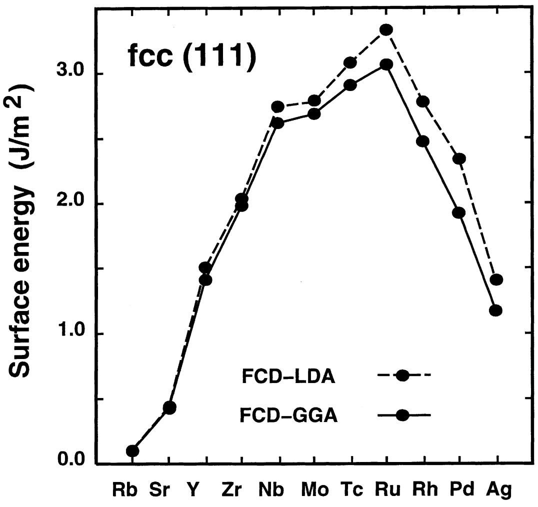

Fig. 3. Comparison of the FCD-LDA and FCD-GGA surface energies for the fcc (111) surface of the 4d metals including Rb and Sr.

Before comparing LDA and GGA results we must address the question of the atomic volume used in the calculations of the surface energy. In the lower panel of Fig. 2 we show the total energy versus Wigner–Seitz radius for a bulk atom ($E^{\rm FCD}_{3D}$) and the energy per atom of the atoms in the surface region ($E^{\rm FCD}_{2D}(N)/N$) of fcc (111) Ru. The difference between these two energies is the surface energy, as defined in Eq. (1), and this is plotted in the upper panel. Inspection of these figures shows that the calculated surface energies depend sensitively on the volume of the underlying bulk lattice and therefore it is important that in the LDA-GGA comparison the calculations are performed at the proper equilibrium volumes. Keeping the volume fixed at the LDA value we find that the mean deviation between the LDA and GGA results along the 4d series including Rb and Sr is about 10%. Repeating the GGA calculations at the GGA equilibrium volumes the mean deviation decreases to 6%. It is the results obtained at the proper LDA and GGA volumes which are plotted in Fig. 3. As one may see, the effect of the GGA over the LDA is rather small for the simple metals, e.g. for Rb and Sr the deviation is 5 and 3%, respectively, which is much lower than the 7–16% found in the jellium calculations, but it

---

[2] The "experimental" values used in the comparison with the jellium surface energy of Ref. [34] were obtained from the experimental values for the corresponding simple metal [1] divided by the corrugation factor of 1.2 as defined in Ref. [35].

increases to approximately 20% in Pd and Ag at the end of the 4d series.

In the comparison between the theoretical fcc (111) surface energies plotted in Fig. 3 and the isotropic values derived from experiment [2] we find that on average the LDA results are 8% larger and the GGA results 7% lower than the experimental results. Therefore, since the GGA yields marginally better surface energies and substantially better atomic equilibrium volumes relative to experiments all the surface energies from the present work presented in Tables 2–8 have been obtained by means of the most recent GGA exchange-correlation functional [29] at the theoretical GGA equilibrium volumes determined in a series of bulk calculations using the same Green's function technique as in the surface calculations.

Finally we note that the effect of the gradient correction to the LDA increases with the roughness and as a consequence reduces the surface energy anisotropy. The effect is found to be about 1% for $\gamma_{100}/\gamma_{111}$, $\gamma_{110}/\gamma_{111}$ in the fcc metals and for $\gamma_{100}/\gamma_{110}$ in the bcc metals.

3. Results and discussion

The present surface energy results are shown in Tables 2–8 in eV atom^{-1} as well as in J m^{-2}. For comparison we also present the available full potential results and two sets of experimentally derived values. All the full potential calculations shown in the tables employ an LDA exchange-correlation functional. Almost all FCD calculations have been performed in the measured low temperature equilibrium crystal structures but in few cases where the α-phase has a lower symmetry than body centered tetragonal (bct) we consider instead a high-pressure phase or a close packed fcc (111) surface. In the tables these structures are indicated by an asterisk. For the hcp metals we have assumed an ideal c/a ratio with the exception

Table 2
Surface energies for the monovalent sp metals calculated by the FCD method in the GGA. For comparison we have included the available full potential and experimental results. The calculated equilibrium lattice constants a are listed in the second column

	Structure (a (Å))	Surface	FCD (eV atom^{-1})	FCD (J m^{-2})	FP (J m^{-2})	Experiment (J m^{-2})
Li	bcc	(110)	0.289	0.556	0.545 [a]	0.522 [b], 0.525 [c]
	(3.431)	(100)	0.383	0.522	0.506 [a]	
		(111)	0.750	0.590	0.623 [a]	
Na	bcc	(110)	0.197	0.253		0.261 [b], 0.260 [c]
	(4.197)	(100)	0.290	0.264		
		(111)	0.546	0.287		
K	bcc	(110)	0.167	0.135		0.145 [b], 0.130 [c]
	(5.300)	(100)	0.249	0.142		
		(111)	0.462	0.152		
Rb	bcc	(110)	0.150	0.104		0.117 [b], 0.110 [c]
	(5.714)	(100)	0.229	0.112		
		(111)	0.417	0.118		
Cs	bcc	(110)	0.142	0.082		0.095 [b], 0.095 [c]
	(6.264)	(100)	0.228	0.093		
		(111)	0.390	0.092		
Fr	bcc	(110)	0.122	0.069		
	(6.320)	(100)	0.202	0.081		
		(111)	0.346	0.080		

[a] Pseudopotential, Ref. [36].
[b] Experimental, Ref. [1].
[c] Experimental, Ref. [2].

Table 3
Surface energies for the divalent sp metals calculated by the FCD method in the GGA. For comparison we have included the available full potential and experimental results. The calculated equilibrium lattice constants a are listed in the second column

	Structure (a (Å))	Surface	FCD (eV atom^{-1})	FCD (J m^{-2})	FP (J m^{-2})	Experiment (J m^{-2})
Ca	fcc	(111)	0.484	0.567		0.502 [a], 0.490 [b]
	(5.624)	(100)	0.535	0.542		
		(110)	0.811	0.582		
Sr	fcc	(111)	0.440	0.428		0.419 [a], 0.410 [b]
	(6.169)	(100)	0.484	0.408		
		(110)	0.725	0.432		
Ba	bcc	(110)	0.464	0.376		0.380 [a], 0.370 [b]
	(5.289)	(100)	0.616	0.353		
		(111)	1.199	0.397		
Ra	bcc	(110)	0.377	0.296		
	(5.372)	(100)	0.515	0.286		
		(111)	1.010	0.324		
Eu	bcc	(110)	0.484	0.485		0.450 [b]
	(4.757)	(100)	0.653	0.463		
		(111)	1.282	0.524		
Yb	fcc	(111)	0.423	0.482		0.500 [b]
	(5.697)	(100)	0.484	0.478		
		(110)	0.721	0.503		
Be	hcp	(0001)	0.495	1.834	1.924 [c], 2.1 [d]	1.628 [a], 2.700 [b]
	(2.236)	$(10\bar{1}0)_A$	1.083	2.126		
		$(10\bar{1}0)_B$	1.626	3.192		
Mg	hcp	(0001)	0.437	0.792	0.641 [e]	0.785 [a], 0.760 [b]
	(3.196)	$(10\bar{1}0)_A$	0.814	0.782		
		$(10\bar{1}0)_B$	1.072	1.030		
Zn	hcp (2.684, $c/a=1.86$)	(0001)	0.385	0.989		0.993 [a], 0.990 [b]
Cd	hcp (3.061, $c/a=1.89$)	(0001)	0.300	0.593		0.762 [a], 0.740 [b]
Hg	hcp* (3.528)	(0001)	0.111	0.165		0.605 [a], 0.575 [b]

[a] Experimental, Ref. [1].
[b] Experimental, Ref. [2].
[c] Full potential LAPW, Ref. [24].
[d] Pseudopotential, Ref. [37].
[e] Pseudopotential, Ref. [38].

of Zn and Cd. For these two elements and for the bct structures we used the experimental [52] c/a ratios listed in the tables.

The theoretical GGA equilibrium lattice constants corresponding to the atomic volumes used in the surface calculations are shown in the second column in the Tables 2–8. The mean deviations between these lattice constants obtained for the low temperature equilibrium crystal structures and the experimental values of Ref. [53] is 2.4% in the case of the simple metals and 1.4%, 1.8%, and 2.1% in the case of the 3d, 4d, and 5d transition metals, respectively. In the determination of the equilibrium volume of the transition metals we included the 3p, 4p, and 5p states in a second energy panel, i.e. treated them as semicore states.

Table 4
Surface energies for the sp metals from Group IIIA–VIA calculated by the FCD method in the GGA. For comparison we have included the available full potential and experimental results. The calculated equilibrium lattice constants *a* are listed in the second column

	Structure (*a* (Å))	Surface	FCD (eV atom^{-1})	FCD (J m^{-2})	FP (J m^{-2})	Experiment (J m^{-2})
Al	fcc	(111)	0.531	1.199	0.939[a]	1.143[b], 1.160[c]
	(4.049)	(100)	0.689	1.347	1.081[a]	
		(110)	0.919	1.271	1.090[a]	
Ga	bct*	(001)	0.376	0.661		0.881[b], 1.100[c]
	(3.018, $c/a=1.58$)	(110)	0.507	0.797		
		(100)	0.695	0.773		
In	bct	(001)	0.342	0.488		0.700[b], 0.675[c]
	(3.352, $c/a=1.52$)	(110)	0.422	0.560		
		(100)	0.632	0.592		
Tl	hcp	(0001)	0.221	0.297		0.602[b], 0.575[c]
	(3.714)	$(10\bar{1}0)_A$	0.494	0.352		
		$(10\bar{1}0)_B$	0.529	0.377		
Sn	bct	(001)	0.387	0.611		0.709[b], 0.675[c]
	(3.187, $c/a=1.83$)	(110)	0.509	0.620		
		(100)	0.716	0.616		
Pb	fcc	(111)	0.226	0.321	0.496[d]	0.593[b], 0.600[c]
	(5.113)	(100)	0.307	0.377		
		(110)	0.513	0.445	0.592[d]	
Sb	sc*	(100)	0.365	0.608		0.597[b], 0.535[c]
	(3.102)	(110)	0.560	0.659		
Bi	sc*	(100)	0.356	0.537		0.489[b], 0.490[c]
	(3.257)	(110)	0.507	0.541		
Po	sc	(100)	0.306	0.437		
	(3.349)	(110)	0.370	0.373		

[a] Pseudopotential, Ref. [39].
[b] Experimental, Ref. [1].
[c] Experimental, Ref. [2].
[d] Pseudopotential, Ref. [26].

However, the inclusion of semicore 3p, 4p, or 5p states in the surface part of the calculations affects the surface energy of the transition metals by less than 2% and therefore these states were considered core states in the surface calculations. A further approximation in the present calculations is the neglect of the relaxation of the atomic positions which may lead to errors of up to a few per cent. As a result we estimate the combined errors in the present surface energies to be 2–5% depending on the surface roughness and 2% in the surface energy anisotropy, both relative to an exact density functional, LDA or GGA, calculation.

3.1. The sp metals

The FCD surface energies of the sp metals for a number of low-index surfaces are presented in Tables 2–4. Since the α-structure of Ga is orthorhombic with 8 atoms in the unit cell the calculations have been performed for the high-pressure bct phase. Furthermore, the α-structure of Sb and Bi may be considered a slightly distorted simple cubic structure and these metals have therefore been treated in the sc structure, while Sn has been calculated in the bct phase of metallic white tin.

The surface energy anisotropies of the monova-

Table 5
Surface energies for the 3d metals calculated by the FCD method in the GGA. For comparison we have included the available full potential and experimental results. The calculated equilibrium lattice constants a are listed in the second column

	Structure (a (Å))	Surface	FCD (eV atom^{-1})	FCD (J m^{-2})	FP (J m^{-2})	Experiment (J m^{-2})
Sc	hcp	(0001)	1.080	1.834		1.275 [a]
	(3.300)	$(10\bar{1}0)_A$	1.694	1.526		
		$(10\bar{1}0)_B$	2.011	1.812		
Ti	hcp	(0001)	1.234	2.632	2.194 [b]	1.989 [c],2.100 [a]
	(2.945)	$(10\bar{1}0)_A$	2.224	2.516		
		$(10\bar{1}0)_B$	2.435	2.754		
V	bcc	(110)	1.312	3.258		2.622 [c],2.550 [a]
	(3.021)	(100)	1.725	3.028	3.18 [d]	
		(211)	2.402	3.443		
		(310)	2.921	3.244		
		(111)	3.494	3.541		
Cr	bcc*	(110)	1.258	3.505		2.354 [c],2.300 [a]
	(2.852)	(100)	2.020	3.979		
		(211)	2.420	3.892		
		(310)	3.030	3.775		
		(111)	3.626	4.123		
Mn	fcc*	(111)	1.043	3.100		1.543 [c],1.600 [a]
	(3.529)					
Fe	bcc	(110)	0.978	2.430		2.417 [c],2.475 [a]
	(3.001)	(100)	1.265	2.222		
		(211)	1.804	2.589		
		(310)	2.153	2.393		
		(111)	2.694	2.733		
Co	hcp	(0001)	0.961	2.775		2.522 [c],2.550 [a]
	(2.532)	$(10\bar{1}0)_A$	1.982	3.035		
		$(10\bar{1}0)_B$	2.476	3.791		
Ni	fcc	(111)	0.695	2.011		2.380 [c],2.450 [a]
	(3.578)	(100)	0.969	2.426		
		(110)	1.337	2.368		
Cu	fcc	(111)	0.707	1.952	1.94 [e]	1.790 [c],1.825 [a]
	(3.661)	(100)	0.906	2.166	1.802 [f]	
		(110)	1.323	2.237		

[a] Experimental, Ref. [2].
[b] Full potential LAPW, Ref. [40].
[c] Experimental, Ref. [1].
[d] Full potential LAPW. In the original paper [41], the authors obtained the following results: ≈5.1 J m^{-2} for the W (100) surface, and ≈3.4 J m^{-2} for the V (100) surface. The results quoted by us contain a correction that appears in the case of thin-film total-energy calculation as was pointed out by Boettger [42].
[e] Full potential LMTO, Ref. [43].
[f] Modified APW, Ref. [44].

lent metals, with the exception of Li, are in good agreement with the results obtained within the jellium model by Perdew [54]. The present GGA calculations yield for Na, K, Rb, and Cs $\gamma_{100}/\gamma_{110}$ in the range from 1.04 to 1.13 compared with 1.14 for the jellium model. The FCD calculation for Li gives $\gamma_{100}/\gamma_{110}=0.94$, which is lower than the corresponding value obtained in the jellium model. On

Table 6
Surface energies for the 4d metals calculated by the FCD method in the GGA. For comparison we have included the available full potential and experimental results. The calculated equilibrium lattice constants *a* are listed in the second column

	Structure (*a* (Å))	Surface	FCD (eV atom^{-1})	FCD (J m^{-2})	FP (J m^{-2})	Experiment (J m^{-2})
Y	hcp	(0001)	1.077	1.506		1.125 [a]
	(3.638)	$(10\bar{1}0)_A$	1.676	1.243		
		$(10\bar{1}0)_B$	2.059	1.527		
Zr	hcp	(0001)	1.288	2.260	2.044 [b], 1.729 [c]	1.909 [d], 2.000 [a]
	(3.248)	$(10\bar{1}0)_A$	2.269	2.111		
		$(10\bar{1}0)_B$	2.592	2.411		
Nb	bcc	(110)	1.320	2.685	2.36 [e], 2.9 [f]	2.655 [d], 2.700 [a]
	(3.338)	(100)	1.987	2.858	2.86 [e], 3.1 [f]	
		(211)	2.410	2.829		
		(310)	3.145	2.861		
		(111)	3.668	3.045		
Mo	bcc	(110)	1.534	3.454	3.14 [e]	2.907 [d], 3.000 [a]
	(3.173)	(100)	2.410	3.837	3.52 [e]	
		(211)	2.738	3.600		
		(310)	3.601	3.626		
		(111)	4.068	3.740		
Tc	hcp	(0001)	1.527	3.691		3.150 [a]
	(2.767)	$(10\bar{1}0)_A$	3.040	3.897		
		$(10\bar{1}0)_B$	3.893	4.989		
Ru	hcp	(0001)	1.574	3.928	3.0 [g], 4.3 [g]	3.043 [d], 3.050 [a]
	(2.723)	$(10\bar{1}0)_A$	3.201	4.236		
		$(10\bar{1}0)_B$	3.669	4.856		
Rh	fcc	(111)	1.002	2.472	2.53 [e]	2.659 [d], 2.700 [a]
	(3.873)	(100)	1.310	2.799	2.81 [e], 2.65 [h], 2.592 [i]	
		(110)	1.919	2.899	2.88 [e]	
Pd	fcc	(111)	0.824	1.920	1.64 [e]	2.003 [d], 2.050 [a]
	(3.985)	(100)	1.152	2.326	1.86 [e], 2.3 [f], 2.130 [j]	
		(110)	1.559	2.225	1.97 [e], 2.5 [f]	
Ag	fcc	(111)	0.553	1.172	1.21 [e]	1.246 [d], 1.250 [a]
	(4.179)	(100)	0.653	1.200	1.21 [e], 1.3 [f], 1.27 [k]	
		(110)	0.953	1.238	1.26 [e] 1.4 [f]	

[a] Experimental, Ref. [2].
[b] Pseudopotential, Ref. [45].
[c] Full potential LAPW, Ref. [40].
[d] Experimental, Ref. [1].
[e] Full potential LMTO, Ref. [5].
[f] Full potential LAPW, Ref. [33].
[g] Pseudopotential, Ref. [46].
[i] Full potential LAPW, Ref. [25].
[h] Pseudopotential, Ref. [47].
[j] Pseudopotential, Ref. [48].
[k] Full potential LAPW, Ref. [49].

the other hand our results for Li are in very good agreement with the pseudopotential calculation by Kokko et al. [36].

For the divalent fcc and bcc metals we find that the surface energy of the second most close packed surface is consistently lower than that of the most

Table 7
Surface energies for the 5d metals calculated by the FCD method in the GGA. For comparison we have included the available full potential and experimental results. The calculated equilibrium lattice constants a are listed in the second column

	Structure (a (Å))	Surface	FCD (eV atom^{-1})	FCD (J m^{-2})	FP (J m^{-2})	Experiment (J m^{-2})
La	hcp*	(0001)	0.909	1.121		1.020 [a]
	(3.873)	$(10\bar{1}0)_A$	1.398	0.915		
		$(10\bar{1}0)_B$	1.690	1.106		
Lu	hcp	(0001)	1.102	1.604		1.225 [a]
	(3.566)	$(10\bar{1}0)_A$	1.845	1.424		
		$(10\bar{1}0)_B$	2.093	1.616		
Hf	hcp	(0001)	1.400	2.472		2.193 [b] ,2.150 [a]
	(3.237)	$(10\bar{1}0)_A$	2.471	2.314		
		$(10\bar{1}0)_B$	2.892	2.709		
Ta	bcc	(110)	1.531	3.084		2.902 [b] ,3.150 [a]
	(3.354)	(100)	2.174	3.097		
		(211)	2.799	3.256		
		(310)	3.485	3.139		
		(111)	4.201	3.455		
W	bcc	(110)	1.806	4.005		3.265 [b] ,3.675 [a]
	(3.196)	(100)	2.955	4.635	4.78 [c]	
		(211)	3.261	4.177		
		(310)	4.338	4.303		
		(111)	4.916	4.452		
Re	hcp	(0001)	1.781	4.214		3.626 [b] ,3.600 [a]
	(2.797)	$(10\bar{1}0)_A$	3.689	4.628		
		$(10\bar{1}0)_B$	4.770	5.985		
Os	hcp	(0001)	1.869	4.566		3.439 [b] ,3.450 [a]
	(2.752)	$(10\bar{1}0)_A$	3.874	5.021		
		$(10\bar{1}0)_B$	4.595	5.955		
Ir	fcc	(111)	1.225	2.971		3.048 [b] ,3.000 [a]
	(3.907)	(100)	1.772	3.722		
		(110)	2.428	3.606		
Pt	fcc	(111)	1.004	2.299	2.067 [d]	2.489 [b] ,2.475 [a]
	(4.019)	(100)	1.378	2.734		
		(110)	2.009	2.819		
Au	fcc	(111)	0.611	1.283	1.04 [e]	1.506 [b] ,1.500 [a]
	(4.198)	(100)	0.895	1.627		
		(110)	1.321	1.700		

[a] Experimental, Ref. [2].
[b] Experimental, Ref. [1].
[c] Full potential LAPW; see footnote d of Table 5.
[d] Pseudopotential, Ref. [50].
[e] Pseudopotential, Ref. [51].

close packed surface, the ratio being approximately 0.96. From Tables 2 and 3 we find that for most of the monovalent and divalent metals, where the two sets of experimentally derived data are close, the relative difference between the experimentally derived and the theoretical results is small. The exception is hcp Be where the experimentally derived values differ considerably among each other. However, in this case the present result for the (0001) surface is in complete agreement with

Table 8
Surface energies for the 5f metals calculated by the FCD method in the GGA. For comparison we have included the available experimental results. The calculated equilibrium lattice constants a are listed in the second column

	Structure (a (Å))	Surface	FCD (eV atom^{-1})	FCD (J m^{-2})	Experiment (J m^{-2})
Ac	fcc	(111)	0.786	0.868	
	(5.786)	(100)	0.764	0.732	
		(110)	1.006	0.681	
Th	fcc	(111)	1.073	1.476	1.500 [a]
	(5.188)	(100)	1.233	1.468	
		(110)	1.722	1.450	
Pa	bct	(110)	1.648	2.902	
	(3.986, $c/a=0.82$)	(100)	2.075	2.584	
		(001)	2.638	2.661	
	fcc*	(111)	1.424	2.302	
	(4.784)				
U	fcc*	(111)	1.367	2.356	1.939 [b], 1.900 [a]
	(4.634)				
Np	fcc*	(111)	1.252	2.208	
	(4.580)				
Pu	fcc*	(111)	1.104	2.007	2.000 [a]
	(4.513)				

[a] Experimental, Ref. [2].
[b] Experimental, Ref. [1].

the first-principles full potential calculations [24,37].

The calculated surface energy anisotropies for the sp metals from groups IIIA–VIA shown in Table 6 are higher than those of the mono- and divalent metals, especially for fcc Pb where a particularly strong facet dependence is found. The anisotropy for Pb is studied experimentally at different temperatures by Heyraud and Metois [3,4] who find that at $T=473$ K $\gamma_{110}/\gamma_{111} \approx 1.06$ which is substantially lower than our result $\gamma_{110}/\gamma_{111}=1.39$ valid at $T=0$ K. To determine the surface energy anisotropy Heyraud and Metois reversed the so-called Wulff construction [55] assuming the surface energy anisotropy to be proportional to the distance from the center to the perimeter of the crystallite. However, this approach neglects entropy effects and cannot yield surface energies for facets which have such a high anisotropy that they are not present in the equilibrium shape at low temperature. For Pb (110) the calculated anisotropy of 1.39 is well beyond 1.22 which is the limit for the existence of a (110) facet at zero temperature and therefore the experimental value of 1.06 for Pb (110) is, at best, a lower boundary.

Our results for fcc Al are slightly higher than those obtained by Schöchlin et al. [39] who applied a slab approach in conjunction with the pseudopotential method. However, Schöchlin et al. used Wigner exchange which for simple metals gives 13–16% lower surface energies [11] than the Ceperley–Alder exchange-correlation functional [28]. We note that the latter functional in the case of Al gives surface energies that differ from the GGA values by less than 2%.

3.2. The transition metals

The FCD surface energies of the 3d, 4d, and 5d transition metals for a number of low-index surfaces are presented in Tables 5–7. In the calculations bcc Fe, hcp Co, and fcc Ni are treated as ferromagnets, i.e. with a spin-polarized exchange-correlation functional [27], while all other metals are treated as paramagnets. For Mn we consider only the close packed fcc (111) surface.

First we compare our FCD results with the other full potential values and from Tables 5–7 we observe that in general the agreement is very good. However, for Ti (0001) and Zr (0001) the LAPW calculation of Ref. [40] gives somewhat lower surface energies than the present method but the surface relaxations, which lowers the surface energy compared with the unrelaxed results, found in Ref. [40] are substantially larger than the experimental values and therefore the LAPW surface energies may be too low. In the case of Ru (0001) the only available pseudopotential calculation [46] lists two very different values for the surface energy, 4.3 and 3.0 J m^{-2}, obtained by different basis sets.

The increase in the surface energy of the transition metals with increasing roughness may be qualitatively understood in terms of the broken bonds model. It may even be described semi-quantitatively by means of a moment expansion of the state density as was done in the pioneering work by Cyrot-Lackmann [56]. As we shall see in Section 3.3, the interactions in a transition metal are quite accurately described by only pairwise interatomic potentials [57,58] and therefore the main contribution to the surface energies of these metals comes from the broken bonds at the semi-infinite surface. Since the number of such broken bonds increases as the surface becomes more open we expect a similar trend in the surface energies. This trend is indeed exhibited by the present results, when expressed in eV atom^{-1}, in perfect agreement with previous studies [5,6]. Owing to a simultaneous increase in surface area, however, this behavior cannot be seen in the surface energies expressed in J m^{-2}.

In the early hcp transition metals the surface energy exhibits a weak orientation dependence and for these elements we find that the $(10\bar{1}0)$ facets are more stable than the most close packed (0001) facets. Furthermore, the surface energies of the $(10\bar{1}0)_B$ facets of the hcp metals from the middle of the series are usually 15–30% larger than those of the $(10\bar{1}0)_A$ facets. Hence, for these metals the $(10\bar{1}0)_B$ facet should not be observed experimentally, or only in a very small fraction compared with the $(10\bar{1}0)_A$ and (0001) facets. The anisotropy of the cubic transition metals will be analyzed in Section 4.

3.3. The light actinides

The FCD surface energies of the light actinides for a few low-index surfaces are presented in Table 8. Since the α-structure of U and Np is orthorhombic with 4 and 8 atoms per unit cell, respectively, and that of Pu is monoclinic with 16 atoms per unit cell we consider here only the close packed fcc (111) surfaces.

For the 5f metals the agreement between the experimentally derived and the theoretical values is very good. The only prior first-principles calculation of the close packed fcc (111) surfaces of the light actinides has been performed by Kollár et al. [7] using an earlier version of the FCD method. The present surface energies of U, Np, and Pu are lower than those of Ref. [7] as a result of the neglect of the higher l charge distribution in the previous work. We note that the effect of the GGA for these surface energies is about 5% compared with the LDA values.

The anisotropies of Ac and Th are very close to those found in the early transition metals. In the case of bct Pa, where the f electrons already play an important role, the most close packed (110) facet appears to be the least stable facet.

4. The equilibrium shape of the crystals

As an example of the application of the database we use the first-principles surface energies to determine the equilibrium shape of crystals of nanometer size. This is the shape that minimizes the total surface energy at constant volume, and at $T=0$ K it is completely determined by the anisotropy of the surface energy [57]. Hence, in the case of weak anisotropy the equilibrium crystal shape is a sphere, while in the case of strong anisotropy it may be a complicated polyhedron.

The equilibrium shape may be determined by the so-called Wulff construction [55], which assumes a complete knowledge of the orientation dependence of the surface energy $\gamma(\mathbf{n})$. In the present application of the Wulff construction for the low-index surfaces we use the first-principles results from the Tables 4–7, and for the high-index surfaces we use a cluster expansion of the total energy based on the low-index first-principles results. In a cluster expansion one expresses the total energy of a given crystal as a linear combination of one-site, two-site, and higher interatomic potentials [58]. It turns out that for transition metal surfaces one needs only to include pairwise interactions to describe the higher-index surfaces with a reasonable accuracy [57]. We therefore apply the expansion

$$\gamma \approx \sum_{s}^{N_s} n_s V_s^{(2)} \tag{2}$$

where n_s is the number of atoms in the coordination shell s, $V_s^{(2)}$ the pair potentials of this shell, and N_s the number of shells considered in the expansion.

In Table 9 we compare for a number of fcc and bcc metals the results obtained by the cluster expansion with the corresponding first-principles results. In these calculations we include two nearest neighbor interactions for the fcc transition metals, i.e. $N_s^{\mathrm{fcc}} = 2$, and four nearest neighbor interactions for the bcc transition metals, i.e. $N_s^{\mathrm{bcc}} = 4$, and find that the relative error in the surface energies of the next higher-index surfaces obtained using the cluster expansion is approximately 2.3%. This relative high accuracy of the cluster expansion observed in the transition metals may be because the coefficients of some two- and multi-site interactions are proportional to the coefficients of the nearest neighour pairwise interactions, and therefore implicitly included in our expansion. The 12.1% relative error for Pb shows that for simple metals the zeroth-order or volume term [58], neglected in Eq. (2), should be taken into account.

The polar plots of the surface energies of Fe, Cu, Mo, Ta, Pt and Pb are shown in Fig. 4. The almost spherical shape of a bcc Ta cluster reflects the weak anisotropy in this metal. In contrast, bcc

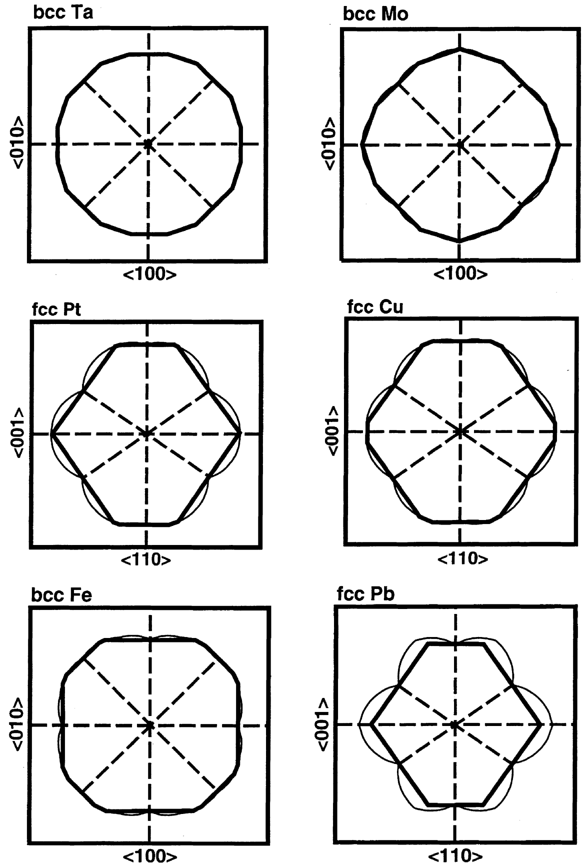

Fig. 4. The calculated equilibrium shape of bcc Ta and Mo clusters in the (001) plane, of fcc Pt and Cu clusters in the (110) plane, and of bcc Fe and fcc Pb clusters in the (001) and (110) planes, respectively. The dashed lines indicate the directions for which first-principles calculations were performed. The thin lines denote the results of the cluster expansion and the heavy lines the theoretical equilibrium crystal shapes.

Table 9
Comparison of the surface energies (in eV atom^{-1} units) calculated using the FCD method and the cluster expansion, Eq. (2)

Method	Pt	Cu	Pb	Ta	Mo	Fe
FCD	2.009	1.323	0.513	4.201	4.068	2.694
Cluster expansion	2.047	1.377	0.458	4.136	4.127	2.613
Percentage error	1.9	3.9	12.1	1.6	1.4	3.1

Mo exhibits a stronger anisotropy and forms in a nearly cubic shape with truncated corners. The equilibrium shape of Pt includes only the (111) and (100) facets. Owing to the relative low value of γ_{110} in Cu a small fraction of the (110) facet is formed. The particular square shape of bcc Fe clusters is a consequence of their ferromagnetic ground state. Thus the magnetic contribution to the surface energy [10] of the (100) Fe surface lowers the surface energy of this facet relative to that of the most close packed (110) surface. As a result, in the equilibrium shape the area of an individual (100) facet is higher than that of a (110) facet. We note that in a paramagnetic calculation the anisotropy is reversed and as a result the equilibrium shape corresponds to that shown in Fig. 4 but rotated by 45°. In recent TEM experiments [59] one finds a shape and orientation of facets in complete agreement with the prediction in Fig. 4.

As a last example we show the equilibrium shape of fcc Pb which on account of the strong anisotropy forms in a slightly distorted hexagonal shape where only the (111) and (001) facets are present. A very similar equilibrium shape without the (110) facet was observed experimentally by Heyraud and Metois [3,4] at T above 473 K, cf. the discussion in Section 3.1.

5. Conclusions

We have calculated a database of low index surface energies for 60 metals which may be used as a starting point for the understanding of a wide range of surface phenomena including faceting, roughening, crystal growth, surface segregation, and the equilibrium shape of mezoscopic crystals. We have taken great care in maintaining a high degree of accuracy and consistency in our computational procedures minimizing possible numerical sources of error. The comparison with available full potential calculations show that our database is accurate. The comparison with surface energies derived from experiments show that the GGA yields result which are marginally better than the LDA. Finally, as an example the database is used to predict the equilibrium shapes of nano-crystals of a few selected metallic elements.

Acknowledgements

The Center for Atomic-scale Materials Physics is sponsored by the Danish National Research Foundation. Part of this work was supported by the research project OTKA 016740 and 23390 of the Hungarian Scientific Research Fund.

References

[1] W.R. Tyson, W.A. Miller, Surf. Sci. 62 (1977) 267.

[2] F.R. de Boer, R. Boom, W.C.M. Mattens, A.R. Miedema, A.K. Niessen, Cohesion in Metals, North-Holland, Amsterdam, 1988.

[3] J.C. Heyraud, J.J. Metois, Surf. Sci. 128 (1983) 334.

[4] J.C. Heyraud, J.J. Metois, Surf. Sci. 177 (1986) 213.

[5] M. Methfessel, D. Henning, M. Scheffler, Phys. Rev. B 46 (1992) 4816.

[6] H.L. Skriver, N.M. Rosengaard, Phys. Rev. B 46 (1992) 7157.

[7] J. Kollár, L. Vitos, H.L. Skriver, Phys. Rev. B 49 (1994) 11288.

[8] A.M. Rodriguez, G. Bozzolo, J. Ferrante, Surf. Sci. 289 (1993) 100.

[9] M. Aldén, H.L. Skriver, S. Mirbt, B. Johansson, Phys. Rev. Lett. 69 (1992) 2296.

[10] M. Aldén, H.L. Skriver, S. Mirbt, B. Johansson, Surf. Sci. 315 (1994) 157.

[11] H.L. Skriver, N.M. Rosengaard, Phys. Rev. B 43 (1991) 9538.

[12] J. Kollár, L. Vitos, H.L. Skriver, Phys. Rev. B 55 (1997) 15353.

[13] L. Vitos, J. Kollár, H.L. Skriver, Phys. Rev. B 55 (1997) 13521.

[14] L. Vitos, J. Kollár, H.L. Skriver, Phys. Rev. B 49 (1994) 16694.

[15] L. Vitos, J. Kollár, H.L. Skriver, Phys. Rev. B 55 (1997) 4947.

[16] R.M. Dreizler, E.K.U. Gross, in: Density Functional Theory, Springer, Berlin, 1990.

[17] O.K. Andersen, O. Jepsen, Phys. Rev. Lett. 53 (1984) 2571.

[18] W.R.L. Lambrecht, O.K. Andersen, Phys. Rev. B 34 (1986) 2439.

[19] O.K. Andersen, O. Jepsen, M. Sob, in: M. Yussouff (Ed.), Electronic Band Structure and its Applications, Springer, Berlin, 1987.

[20] O.K. Andersen, O. Jepsen, G. Krier, in: V. Kumar, O.K. Andersen, A. Mookerjee (Eds.), Methods of Electronic

Structure Calculations, World Scientific, Singapore, 1994, pp. 63.
[21] O.K. Andersen, Z. Pawlowska, O. Jepsen, Phys. Rev. B 34 (1986) 5253.
[22] L. Vitos, J. Kollár, H.L. Skriver, in: A. Gonis, P.E.A. Turchi, J. Kudrnovsky (Eds.), NATO ASI Series B: Physics, Stability of Materials, Plenum, New York, 1996, p. 393.
[23] B. Wenzien, J. Kudrnovsky, V. Drchal, M. Sob, J. Phys.: Condens. Matter 1 (1989) 9893.
[24] P.J. Feibelman, Phys. Rev. B 46 (1992) 2532.
[25] P.J. Feibelman, D.R. Hamann, Surf. Sci. 234 (1990) 377.
[26] M. Mansfield, R.J. Needs, Phys. Rev. B 43 (1991) 8829.
[27] J. Perdew, Y. Wang, Phys. Rev. B 45 (1992) 13244.
[28] D.M. Ceperley, B.J. Alder, Phys. Rev. Lett. 45 (1980) 566.
[29] J.P. Perdew, K. Burke, M. Ernzerhof, Phys. Rev. B 77 (1996) 3865.
[30] S.L. Cunningham, Phys. Rev. B 10 (1974) 4988.
[31] L. Vitos, J. Kollár, Phys. Rev. B 51 (1995) 4074.
[32] J. Perdew, A. Zunger, Phys. Rev. B 23 (1981) 5048.
[33] M. Weinert, R.E. Watson, J.W. Davenport, G.W. Fernando, Phys. Rev. B 39 (1989) 12585.
[34] J.P. Perdew, J.A. Chevary, S.H. Vosko, K.A. Jackson, M.R. Pederson, D.J. Singh, C. Fiolhais, Phys. Rev. B 46 (1992) 6671.
[35] J.P. Perdew, Y. Wang, E. Engel, Phys. Rev. Lett. 66 (1991) 508.
[36] K. Kokko, P.T. Salo, R. Laihia, K. Mansikka, Surf. Sci. 348 (1996) 168.
[37] R. Yu, P.K. Lam, Phys. Rev. B 39 (1989) 5035.
[38] A.F. Wright, P.J. Feibelman, S.R. Atlas, Surf. Sci. 302 (1994) 215.
[39] J. Schöchlin, K.P. Bohnen, K.M. Ho, Surf. Sci. 324 (1995) 113.
[40] P.J. Feibelman, Phys. Rev. B 53 (1996) 13740.
[41] C.L. Fu, S. Ohnishi, H.J.F. Jansen, A.J. Freeman, Phys. Rev. B 31 (1985) 1168.
[42] J.C. Boettger, Phys. Rev. B 49 (1994) 16798.
[43] H.M. Polatoglou, M. Methfessel, M. Scheffler, Phys. Rev. B 48 (1993) 1877.
[44] H. Bross, M. Kauzmann, Phys. Rev. B 51 (1995) 17135.
[45] M. Yamamoto, C.T. Chan, K.M. Ho, Phys. Rev. B 50 (1994) 7932.
[46] M.Y. Chou, J.R. Chelikowsky, Phys. Rev. B 35 (1987) 2124.
[47] I. Morrison, D.M. Bylander, L. Kleinman, Phys. Rev. Lett. 71 (1993) 1083.
[48] A. Wachter, K.P. Bohnen, K.M. Ho, Surf. Sci. 346 (1996) 127.
[49] H. Erschbaumer, A.J. Preeman, C.L. Fu, R. Podloucky, Surf. Sci. 243 (1991) 317.
[50] P.J. Feibelman, Phys. Rev. B 52 (1995) 16845.
[51] N. Takeuchi, C.T. Chan, K.M. Ho, Phys. Rev. B 43 (1991) 13899.
[52] P. Villars, L.D. Calvert (Eds.), Pearson's Handbook of Crystallographic Data for Intermetallic Phases, Materials Park, OH, 1991.
[53] D.A. Young, Phase Diagrams of the Elements, University of California Press, Berkeley, CA, 1991.
[54] J.P. Perdew, Prog. Surf. Sci. 48 (1995) 245.
[55] See e.g. M.C. Desjonquères, D. Spanjaard, Concepts in Surface Physics, Springer, Berlin, 1996.
[56] F. Cyrot-Lackmann, Surf. Sci. 15 (1969) 535.
[57] S. Wei, M.Y. Chou, Phys. Rev. B 50 (1994) 4859.
[58] J.A. Moriarty, R. Phillips, Phys. Rev. Lett. 66 (1991) 3036.
[59] L. Theil Hansen, personal communication.